文章编号：1001-9014(2024)06-0733-05

DOI:10.11972/j.issn.1001-9014.2024.06.001

Enhancement of mid-wavelength infrared absorbance by alkane-grafted $Ti_3C_2T_x$ MXene thin-films

ZHAO Zhen-Yu[1*], KITAHARA Hideaki[2], ZHANG Chen-Hao[3], TANI Masahiko[2]

(1. Department of Physics, Shanghai Normal Univeristy, Shanghai 200234, China;
2. Research Center for Development of Far-Infrared Region, University of Fukui, Fukui 910-8507, Japan;
3. Department of Chemistry, Shanghai Normal Univeristy, Shanghai 200234, China)

Abstract: An enhancement of mid-wavelength infrared absorbance is achieved via a cost-effectively chemical method to bend the flakes by grafting two types of alkane octane (C_8H_{18}) and dodecane ($C_{12}H_{26}$) onto the surface terminals respectively. The chain-length of alkane exceeds the bond-length of surface functionalities T_x (=O, -OH, -F) so as to introduce intra-flake and inter-flake strains into $Ti_3C_2T_x$ MXene. The electronic microscopy (TEM/AFM) shows obvious edge-fold and tensile/compressive deformation of flake. The alkane termination increases the intrinsic absorbance of $Ti_3C_2T_x$ MXene from no more than 50% up to more than 99% in the mid-wavelength infrared region from 2.5 μm to 4.5 μm. Such an absorption enhancement attributes to the reduce of infrared reflectance of $Ti_3C_2T_x$ MXene. The C-H bond skeleton vibration covers the aforementioned region and partially reduces the surface reflectance. Meanwhile, the flake deformation owing to edge-fold and tensile/compression increases the specific surface area so as to increase the absorption as well. These results have applicable value in the area of mid-infrared camouflage.

Key words: mid-wavelength infrared, MXene, infrared absorption, optical properties of thin-film

烷基修饰碳化钛MXene薄膜中波红外吸收增强效应

赵振宇[1*]，北原英明[2]，张宸豪[3]，谷正彦[2]

(1. 上海师范大学 物理系，上海 200234；
2. 福井大学 远红外区域开发研究中心，福井910-8507，日本；
3. 上海师范大学 化学系，上海200234)

摘要：本文介绍了一种具有低成本高效益的化学方法，通过将辛烷(C_8H_{18})和十二烷($C_{12}H_{26}$)两种类型的烷烃基团分别嫁接到MXene表面，实现对薄片的弯曲形变，从而增强了中波长的红外吸光度。烷烃的链长超过表面官能团T_x(=O、-OH、-F)的键长，从而将片内应力和片间应力作用到$Ti_3C_2T_x$ MXene薄片表面。电子显微镜和原子力显微镜测试表明，薄片有明显的边缘褶皱和拉伸/压缩变形。薄片终端的烷烃将$Ti_3C_2T_x$ Mxene从2.5 μm到4.5 μm波长的中波红外区域的吸光度由略高于50%，提高到99%以上。这种吸收增强归因于$Ti_3C_2T_x$ MXene红外反射率的降低。C-H键骨架振动覆盖了上述区域，并部分降低了表面反射率。同时，由于边缘褶皱和拉伸/压缩导致的薄片变形增加了比表面积，从而增加了吸收。此结果对中波红外伪装技术具有一定的应用价值。

关　键　词：中波红外；MXene；红外吸收；薄膜的光学特性

中图分类号：O472.3　　**文献标识码**：A

Introduction

The mid-wavelength region from 3 μm to 5 μm portion of infrared radiation band (IR), is an atmospheric window for IR seekers to detect the infrared signature of object[1]. It gives a rise to a great deal of application such as night vision, thermography, remote control, molecu-

Received date: 2024-02-20, **revised date**: 2024-04-08　　**收稿日期**：2024-02-20，**修回日期**：2024-04-08

Biography: ZHAO Zhen-Yu(1980-), male, Shanghai, associate researcher. Research area involves infrared and terahertz physics and technology.
* **Corresponding author**: E-mail: zyzhao@shnu.edu.cn

lar spectroscopy, climatology and meteorology, etc[1]. An infrared signature depends on many factors, including the shape and size of the object[2], temperature[3], emissivity, reflection of external sources (earthshine, sunshine, skyshine) from the object's surface[4], the background against which it is viewed[5] and the waveband of the detecting sensor. Due to the requirement of national defense and border security, any technique reducing infrared signature of significant objects is helpful to avoid the attack by infrared guided weapons and infrared surveillance sensors[6-7], and thus increases the object overall survivability. Aforementioned demands stimulates continuous interests in seeking for mid-wavelength infrared absorbing materials.

Two-dimensional transition metal carbides and nitrides (MXenes) have shown diverse light-matter interactions in a broad frequency range[8], owing to their highly anisotropic electronic and optical properties, easy-to-functionalize surfaces, and high density of states at the Fermi level[8]. For instance, The absorption rate of the 15 μm thick $Ti_3C_2T_x$ film in the visible light range (380-780 nm) is around 90%, while it decreases rapidly in the near-infrared range (1-3 μm), reaching a minimum of ~10% in the mid-infrared range[9]. Li et al. placed thin film materials such as MXene, graphene, graphene oxide, montmorillonite and stainless steel on a high-temperature substrate (508 ℃), and the measured radiation temperatures were 181 ℃, 223 ℃, 294 ℃, 421 ℃ and 159 ℃ respectively[10]. As such, $Ti_3C_2T_x$ exhibits excellent low infrared radiation characteristics. Deng et al. combined the concept of multi-color printing and printed $Ti_3C_2T_x$ solutions with different infrared emissivities into composite anti-counterfeiting patterns, so that the infrared anti-counterfeiting patterns can be identified and decrypted with the help of a thermal image camera[11]. In the solid solution of MXene, precise control of infrared emissivity from low to high can be through changes in composition and atomic structure. In addition, utilizing the electrochemical properties of MXene, the electrochemically driven infrared emissivity can be controlled by applying an external electric field[12]. This shows that MXene has huge application potential in the fields of optical communication, imaging, and thermal management in the infrared band, and that the surface plasmons of MXene can be controlled through MXene components, surface groups, and film thickness. Utilizing these properties of MXene for metasurface design promises new breakthroughs. However, there are currently few reports on the basic dielectric properties of different types of MXenes in the infrared band, and further exploration is urgently needed.

In this work, we present a chemical method to deform the MXene flakes locally by grafting two types of alkane octane (C_8H_{18}) or dodecane ($C_{12}H_{26}$) on the lattice-site of terminated functional group of $Ti_3C_2T_x$ MXene. Then, MXene thin-film is achieved by the drop-cast process. The atomic force microwscopy (AFM) in combination with transmission electronic microscopy (TEM) and scanning electronic microscopy (SEM) reveal the morphological change of $Ti_3C_2T_x$ MXene. The mid-wavelength IR absorption of $Ti_3C_2T_x$ MXene and alkane grafted ones are tested by Fourier transform infrared spectroscopy (FT-IR). Correspondingly, IR absorption enhancement owing to flake-curvature of alkane grafted $Ti_3C_2T_x$ MXene thin-film are discussed.

1 Experiments

The $Ti_3C_2T_x$ MXene is synthesized by a top-down method of chemical exfoliation. All the chemicals are purchased from Sigma-Aldrich® Lab & Production Materials of Merck Ltd. Figure 1 shows the schematic diagram of the flakes of $Ti_3C_2T_x$, $Ti_3C_2T_x$-C_8H_{18}, $Ti_3C_2T_x$-$C_{12}H_{26}$ MXene. First, the 0.5 g of Ti_3AlC_2 MAX phase precursor was added into a mixture of deionized (DI) water (13.5 mL)/ HF (3 mL), and stirred at room temperature for 24 hours. The sediment is washed with DI water several times until the pH value reached neutral, which is then added into 15 mL DI water containing 1.5 g of LiCl under vigorous stirring at room temperature for 12 hours. The monolayer $Ti_3C_2T_x$ suspension is washed with DI water several times and collected by centrifugation at 3 500 rpm for 5 min. Second, centrifuged the prepared single-layer or few-layer $Ti_3C_2T_x$ solution at high speed and took out 1g sediment after the solvent was completely removed. Separately added DI water (10 ml), ethanol (160 ml), and aqueous ammonia(15 ml), the mixed solution was fully stirred for 24 hours. Then, 1 ml of (octyl)-triethoxysiloxane (OTES) was introduced into the above solution and stirred vigorously for 24 hours again. After the reaction was finished, de-ionized water and ethanol were used for centrifugal cleaning in turn to obtain hydrophobic $Ti_3C_2T_x$-C_8H_{18} MXene flakes. Third, centrifuged the prepared mono-layer $Ti_3C_2T_x$ solution at high speed and took out 1 g sediment after the solvent was completely removed. Separately added DI water (10 ml), ethanol (160 ml), and aqueous ammonia (15 ml), the mixed solution was stirred for 24 hours. Then, 1 ml of (dodecyl)-triethoxysiloxane (DCTES) was introduced into the above solution and stirred vigorously for 24 hours again. After the reaction was finished, de-ionized water and ethanol were used for centrifugal cleaning in turn to obtain hydrophobic $Ti_3C_2T_x$-$C_{12}H_{26}$ flakes.

The MXene thin films are achieved by drop-cast and spin-coating process. The polyimide substrate was pre-ultrasonically cleaned with ethanol and de-ionized water for 20 min. Aforementioned MXene flakes are dripped onto a 75 μm thick polyimide (Du Pont® Kapton™ HN) membrane of 20×15 mm area and spin-coating for 30 seconds at 500 rmp first followed by 15 seconds at 1500 rmp later. The as-fabricated MXene thin-film is shown in Fig. 1 (b). The MXene specimen is in the x-y plane, and the incident IR radiation is along the z axis. The transmittance spectra of the MXene were measured by an FT-IR system (JASCO FT/IR-660 plus) with 1 cm^{-1} resolution. The scanning range is from 2.5 μm to 4.5 μm. The diameter of terahertz focal area is 1 mm, which is much smaller than the thin-film size. All the measured transmittance and reflection spectra of as-fabricated MXene thin films

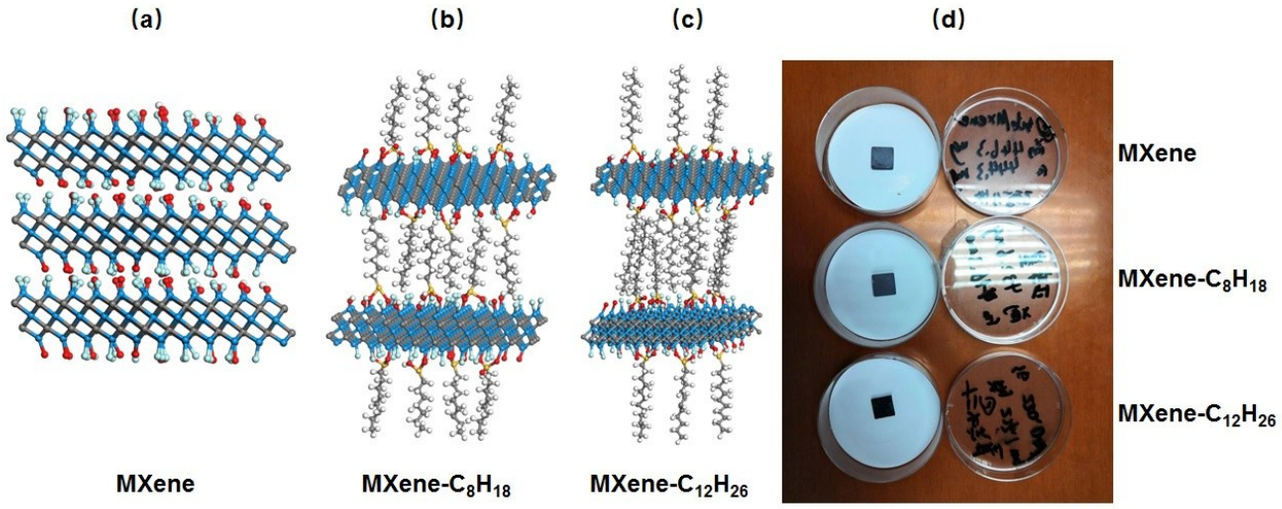

Fig. 1 The schematic diagram of the flakes of (a) $Ti_3C_2T_x$; (b) $Ti_3C_2T_x$-C_8H_{18}; (c) $Ti_3C_2T_x$-$C_{12}H_{26}$ MXene (blue solid-ball: titanium; grey solid-ball: carbon; white solid-ball: hytrogen; red solid ball: fluorine; cyan solid ball: Oxygen); (d) image of as-fabricated $Ti_3C_2T_x$, $Ti_3C_2T_x$-C_8H_{18}, $Ti_3C_2T_x$-$C_{12}H_{26}$ MXene thin-film
图 1 (a) $Ti_3C_2T_x$;(b) $Ti_3C_2T_x$-C_8H_{18};(c) $Ti_3C_2T_x$-$C_{12}H_{26}$ MXene薄片示意图(蓝色实心球:钛;灰色实心球:碳;白色实心球:氢;红色实心球:氟;天蓝色实心球:氧);(d) $Ti_3C_2T_x$, $Ti_3C_2T_x$-C_8H_{18}, $Ti_3C_2T_x$-$C_{12}H_{26}$ Mxene薄膜的制备图像

are automatically calculated to remove the background signals. The morphology of MXene nano-flakes is captured by Zeiss® Gemini™ 500 SEM. To prevent unwanted discharge, a thin carbon layer is sputtered on the surface of the MXene thin-film by a Safematic® CCU-010 HV high compact vacuum coating system. Images were obtained by a secondary electron detector, with a working distance of about 5 mm and a 5 kV acceleration voltage. The detailed images on the lateral edge of as-fabricated MXene nano-flakes are recorded by Thermo Scientific Talos™ transmission electron microscope (TEM). The AFM microscopy was performed on Smart SPM by AIST-NT. Diluted MXene nano-flakes are dispersed onto the mica plate for AFM measurement. X-ray photoelectron spectroscopy (XPS) was performed on a X-ray photoelectron spectrometer (Thermo fisher Scientific, K-Alpha, USA) apparatus using an Al Kα X-ray source to investigate their surface electronic states.

2 Results and discussions

The morphology of as-fabricated MXene flakes is conducted by AFM and SEM and TEM respectively. Figure 2(a) shows the $Ti_3C_2T_x$, $Ti_3C_2T_x$-C_8H_{18}, $Ti_3C_2T_x$-$C_{12}H_{26}$ MXene flakes are dissolved in the aquesous solution. As such, one can find out the single flakes obviously. The surface roughness of single flakes are measured by the AFM shown in Fig. 2(b). The alkane grafting increase the surface roughness of single flakes of $Ti_3C_2T_x$ MXene. Figure 2(c) shows the cross-section of drop-casted MXene thin-films. The average thickness of all the thin-film is about (15±5) μm. The detailed surface morphology of $Ti_3C_2T_x$, $Ti_3C_2T_x$-C_8H_{18}, $Ti_3C_2T_x$-$C_{12}H_{26}$ MXene flakes are shown in Fig. 2(d).

An obvious boundary exists in between the adjacent flakes of $Ti_3C_2T_x$ MXene. A zoom-in insight on the flake shape shows straight lineshaped boundary of the flakes. However, the assembly of $Ti_3C_2T_x$-C_8H_{18} and $Ti_3C_2T_x$-$C_{12}H_{26}$ flakes mono-sheets seems to be crumpled shapes with numerous ridges and rough surface. Such a wrinkled morphology of $Ti_3C_2T_x$ flakes is due to alkane grafting. A zoom-in insight on the flake shape shows curved grain-boundary of the flakes. Meanwhile, the whole flakes mono-sheet seems to be in tensile or compressive deformation. Especially, the lateral edge of $Ti_3C_2T_x$-$C_{12}H_{26}$ exhibits folds along the lateral edge compared to the local lateral edge spikes of $Ti_3C_2T_x$-C_8H_{18} MXene flakes. A deep insight on the curved deformation are achieved by TEM at nanometer scale, of which the electrons beam is focused on the lateral edge of aforementioned MXene flakes. As shown in Fig. 2, the edge of $Ti_3C_2T_x$ MXene is flat, while the lateral edge of $Ti_3C_2T_x$-C_8H_{18} flakes is obviously folded. To the $Ti_3C_2T_x$-$C_{12}H_{26}$ flakes, a stronger edge-folding almost wrap up the flakes from the corner. Such a curvature introduced into 2D mono-sheet flakes changes the spatial distribution of strain so as to increase the roughness of MXene thin-film. This phenomenon is similar to the textured graphene of curved-flakes. Compared to a planar surface, a rough surface has a higher specific surface area according to the Brunauer - Emmett - Teller (BET) theory[13].

Since the MXene speciemen are coated with carbon for SEM measurement, the carbon ratio has to be excluded. Hytrogen is too light to be recorded in our EDS measurement. The aluminium is the residue of MAX phase precursor. Interestingly, the surface functional element T_x (-F, -O) oxygen-fluorine ratio (O:F) is changed from 2:1 ($Ti_3C_2T_x$) up to 4:1 ($Ti_3C_2T_x$-C_8H_{18}) and 7:1 ($Ti_3C_2T_x$-$C_{12}H_{26}$). As such, the alkanes occupy the atomic site of flurione so as to be grafted onto the surface of $Ti_3C_2T_x$ MXene nano-flakes. Oxygen termination plays a significant role in bridging nearby titanium between the $Ti_3C_2T_x$ MXene nano-flakes. However, both C_8H_{18} and

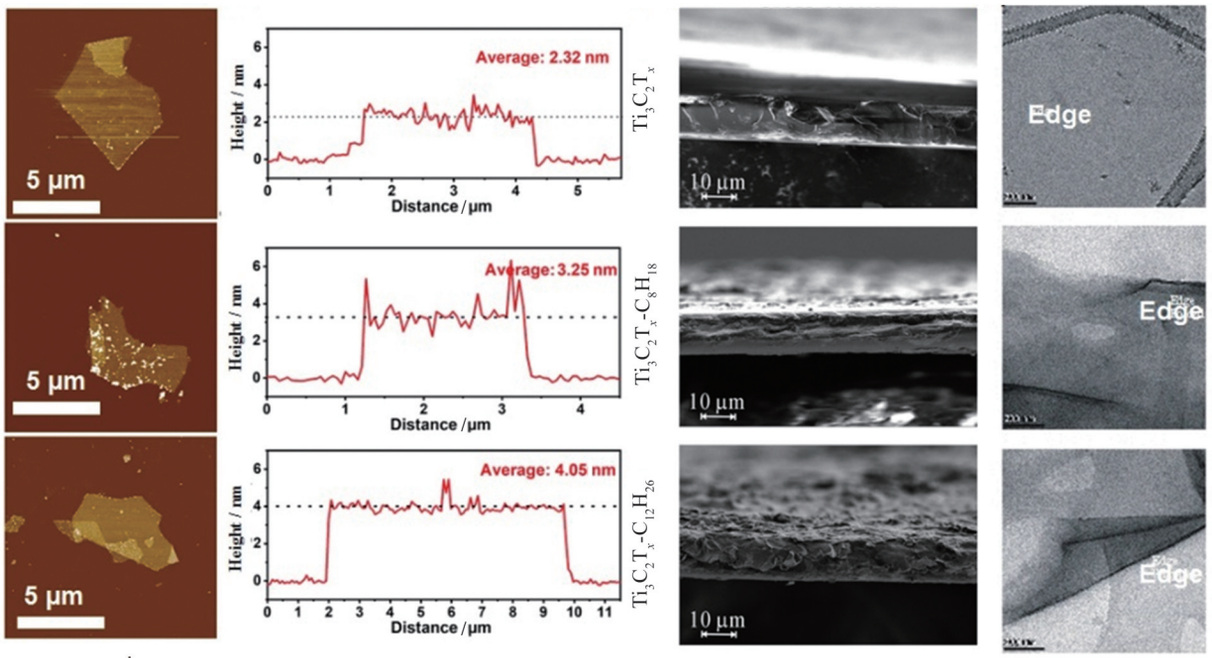

Fig. 2 (a) The AFM image of the flakes of $Ti_3C_2T_x$, $Ti_3C_2T_x$-C_8H_{18}, $Ti_3C_2T_x$-$C_{12}H_{26}$ MXene; (b) the surface roughness of corresponding MXene flakes; (c) SEM cross-sections of $Ti_3C_2T_x$, $Ti_3C_2T_x$-C_8H_{18}, $Ti_3C_2T_x$-$C_{12}H_{26}$ MXene thin-films; (d) TEM image of as-fabricated MXene thin-film

图2 (a) $Ti_3C_2T_x$, $Ti_3C_2T_x$-C_8H_{18}, $Ti_3C_2T_x$-$C_{12}H_{26}$ MXene薄片的AFM图像;(b)相应的MXene薄片的表面粗糙度;(c) $Ti_3C_2T_x$, $Ti_3C_2T_x$-C_8H_{18}, $Ti_3C_2T_x$-$C_{12}H_{26}$ 薄膜的SEM横截面;(d)制备的MXene薄膜的TEM图像

Table 1 Elementary analysis of MXene (Atom %)
表 1 MXene的元素分析(原子 %)

MXene	Ti	O	F	Al
$Ti_3C_2T_x$	64.2	21.2	11.1	0.16
$Ti_3C_2T_x$ -C_8H_{18}	56.6	29.3	7.35	0.25
$Ti_3C_2T_x$ -$C_{12}H_{26}$	35.6	49.3	6.98	0.22

$C_{12}H_{26}$ are straight-chain alkanes, of which the carbon-chain length is much longer than the oxygen bond length. As such, the alkane on the surface of one MXene nano-flake forms interlayer repulsion opposite to the force of oxygen bond resulting in a compressive/tentile deformation of alkane-grafted $Ti_3C_2T_x$ MXene as well as the edge-folding effect.

The IR transmission and reflection spectra of the as-fabricated $Ti_3C_2T_x$ MXene thin-film are presented in Fig. 3. Clearly, The transittance of $Ti_3C_2T_x$ MXene, $Ti_3C_2T_x$-C_8H_{18} and $Ti_3C_2T_x$-$C_{12}H_{26}$ MXene are almost close to the lowest detection limit of FT-IR since there is only background noise. However, the reflection spectra of as-fabricated $Ti_3C_2T_x$ MXene thin-film shows a distinct larger reflectance than the other two types of alkane-grafted MXenes, which is presented in Fig. 3. The reflectance of $Ti_3C_2T_x$ MXene is from 45% to 70% in the wavelength range from 2 μm to 4.8 μm. However, that of $Ti_3C_2T_x$-C_8H_{18} MXene is below 3%, while that of $Ti_3C_2T_x$-$C_{12}H_{26}$ MXene is even below 1%. All the as-fabricated $Ti_3C_2T_x$ MXene thin-film shows a climbing behavior in the reflection spectrum as a function of wavelength. It can be found that the reflection ratio decreases at a factor of 10 in the entire spectrum. According to the optics principle, the strong attenuation of transmittance and reflectance implies a dramatically increase of optical absorption in measurement, which obeys the regulation as below[13]:

$$A = 1 - T - R \quad , \quad (1)$$

where R, A, and T are the fractions of the power which are reflected, absorbed, and transmitted correspondingly. Therefore, the optical absorption of samples can be extracted from Eq. (1), as illustrated in Fig. 3.

The IR absorption of intrinsic $Ti_3C_2T_x$ MXene is from 55% to 29% with the wavelength increasing from from 2 μm to 4.8 μm. However, the IR absorption of $Ti_3C_2T_x$-C_8H_{18} and $Ti_3C_2T_x$-$C_{12}H_{26}$ MXene are both beyond 99%. The slope of the IR absorption function of intrinsic $Ti_3C_2T_x$ MXene decreases with the wavelength climbing up. To the $Ti_3C_2T_x$-C_8H_{18} and $Ti_3C_2T_x$-$C_{12}H_{26}$ MXene, however, their IR spectra becomes very much flat compared to that of the intrinsic $Ti_3C_2T_x$ MXene. At this point, one can summarize that the alkane graft enhances the IR absorbance by reducing the reflectance of MXene thin-film. The origin of absorption enhancement can be revealed from the morphologic graphics. The flake tensile or compressione as well as the edge-folding of the flakes enlarge the specific surface area for IR absorption, which enhances the effective area for the interaction of IR photon and MXene. These curvature increase the surface roughness inducing a diffusion reflection, which is responsible for the energy loss of specular reflection. Furthermore, the skeleton molecular vibration of carbon-chain maybe

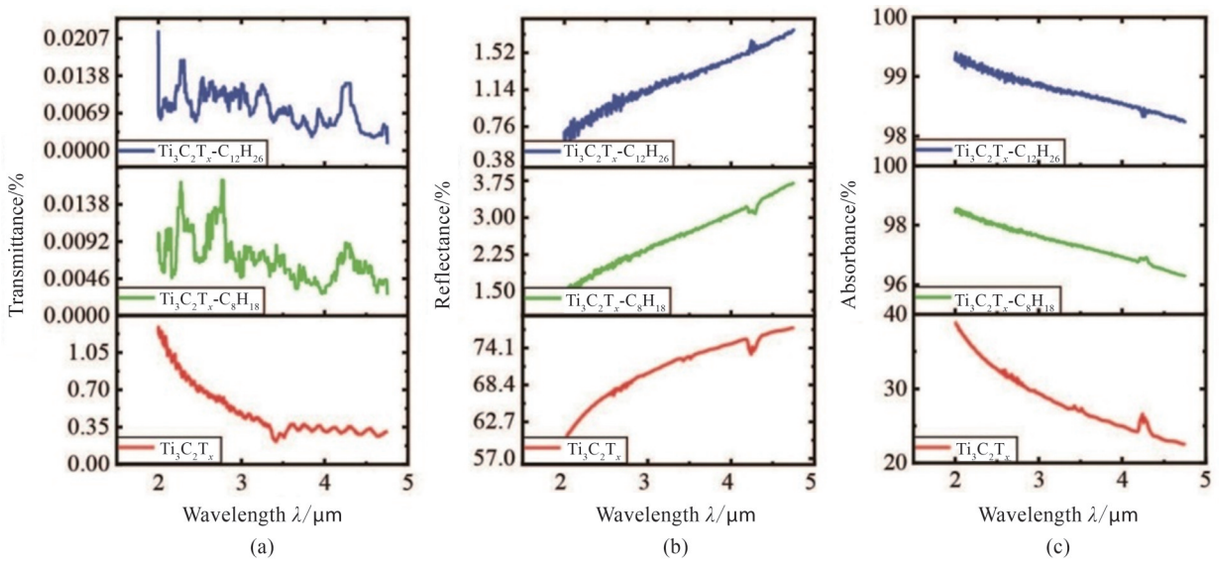

Fig. 3 (a) Transmission spectra; (b) reflection spectra; (c) absorption spectra of $Ti_3C_2T_x$, $Ti_3C_2T_x$-C_8H_{18}, $Ti_3C_2T_x$-$C_{12}H_{26}$ MXene. (red solid-line: $Ti_3C_2T_x$; MXene; green solid-line: $Ti_3C_2T_x$-C_8H_{18} MXene; blue solid-line: $Ti_3C_2T_x$-$C_{12}H_{26}$ MXene)
图3 $Ti_3C_2T_x$, $Ti_3C_2T_x$-C_8H_{18}, $Ti_3C_2T_x$-$C_{12}H_{26}$ Mxene的(a)透射谱;(b)反射谱;(c)吸收谱(红色实线:$Ti_3C_2T_x$;绿色实线:$Ti_3C_2T_x$-C_8H_{18};蓝色实线:$Ti_3C_2T_x$-$C_{12}H_{26}$)

contribute to the enhancement of absorption at mid-wavelength infrared region. The spectra of simple alkanes are characterized by absorptions due to C-H stretching and bending The IR spectrum of octane is shown strong bands in the 3 000-2 850 cm^{-1} region due to C-H stretch. The C-H scissoring (1 470 cm^{-1}), methyl rock (1 383 cm^{-1}), and long-chain methyl rock (728 cm^{-1}) are noted on this spectrum[14]. All these vibration are locate in the mid-wavelength infrared region froms 3 μm to 5 μm. Since most organic compounds have these features, these C-H vibrations are usually not noted when interpreting a routine IR spectrum. However, the C=C stretching and bending bands are either too weak or of a too low frequency to be detected in IR spectroscopy.

3 Conclusions

The versatility of MXenes at infrared wavelengths provides a platform for developing MXene-based smart, flexible devices and wearables capable of selective and localized thermal management, aiming at radiative heating/cooling, IR identification, photothermal conversion, and thermal imaging. Alkane graft increases the absorbance of MXene by reducing the reflectance. The edge-folding of the alkane decorated MXene increases the specific surface area, which contribute to the enhancement of absorption at mid-wavelength infrared region. The skeleton molecular vibration of carbon-chain maybe contribute to the enhancement of absorption at mid-wavelength infrared region.

References

[1] Booth N, Smith A S. Infrared Detectors [M]. Goodwin House Publishers, New York & Boston, 1997, 241-248
[2] Munir F, Azam S, Rafique M A, *et al*. Exploring thermal images for object detection in underexposure regions for autonomous driving [J]. *Applied Software Computing*, 2023, **121**: 108793.
[3] Altay F, Velipasalar S. The use of thermal cameras for pedestrian detection [J]. *IEEE Sensors Journal*, 2022, **22**: 11489-11498.
[4] Yu B, Chen Y, Cao S Y. Three-channel infrared imaging for object detection in Haze [J]. *IEEE Transactions on Instrumentation and Measurement*, 2022, **71**: 5008513.
[5] Razeghi M, Nguyen B M. Advances in mid-infrared detection and imaging: a key issues review [J]. *Report on Progress in Physics*, 2014, **77**: 082401.
[6] Li J, Dehzangi A, Brown G, *et al*. Mid-wavelength infrared avalanche photodetector with AlAsSb/GaSb superlattice [J]. *Scientific Reports*, 2021, **11**: 7104.
[7] Tournié E, Cerutti L. Mid-infrared Optoelectronics [M]. Woodhead Publishing Press, 2020, 200-265.
[8] Han M, Zhang D, Singh A, *et al*. Versatility of infrared properties of MXenes [J]. *Materials Today*, 2023, **64** (1): 31-39.
[9] Li Y, Xiong C, Huang H, *et al*. 2D $Ti_3C_2T_x$ MXenes: visible black but infrared white materials [J]. *Advanced Materials*, 2021, **33** (41): 2103054.
[10] Li L, Shi M K, Liu X Y, *et al*. Ultrathin titanium carbide (MXene) films for high-temperature thermal camouflage [J]. *Advanced Functional Materials*, 2021, **31**(2): 2101381.
[11] Deng Z, Li L, Tang P, *et al*. Controllable surface-grafted MXene inks for electromagnetic wave modulation and infrared anti-counterfeiting applications [J]. *ACS Nano*, 2022, **16**(10): 16976 - 16986.
[12] Lu F, Shi D, Tan P, *et al*. A novel infrared electrochromic device based on $Ti_3C_2T_x$ MXene [J]. *Chemical Engineering Journal*, 2022, **450**(4): 138324.
[13] Brunauer S, Emmett P H, Teller E. Adsorption of gases in multimolecular layers [J]. *Journal of the American Chemical Society*, 1938, **60** (2): 309 - 319.
[14] Tang X, Li Y, Zhu L, *et al*. On-line multi-component alkane mixture quantitative analysis using Fourier transform infrared spectrometer [J]. *Chemometrics and Intelligent Laboratory Systems*, 2015, **146**: 371-377.